Orientation-shape coupling between liquid crystal and membrane through the anchoring effect

Shun Okushima* and Toshihiro Kawakatsu
Department of Physics, Graduate School of Science, Tohoku University, Sendai 980-8578, Japan
(Received 7 February 2017; revised manuscript received 1 October 2017; published 28 November 2017)

We perform a series of Monte Carlo simulations on an interface between a liquid crystal (LC) material in isotropic phase in its bulk and a surfactant membrane. These two objects are simulated using coarse-grained molecular models. We estimate physical properties of the membrane such as the interfacial tension and the bending rigidity, focusing on the anchoring effects of the membrane on the LC. According to our simulation results, when the strength of the homeotropic anchoring denoted by the anchoring parameter ξ is increased, the interfacial tension decreases and the bending rigidity first increases in $\xi < \xi_{\mathrm{m}}$, and it then decreases in $\xi_{\mathrm{m}} < \xi$. We explain these results by constructing a continuum field model based on the two order parameters: directional order of LC and the membrane shape. These order parameters are mutually interacting through the anchoring effect, the fluctuation coupling between the LC and the membrane, and the effect of the nematic layer.

DOI: 10.1103/PhysRevE.96.052704

I. INTRODUCTION

Liquid crystals (LCs) have versatile photonic properties originating from the anisotropy in their molecular shapes and in their dielectric constants [1]. Due to such properties, LCs are utilized in many electro-optical devices such as displays. Recent research has suggested a possible use of LCs in molecular detection techniques for biomolecules by taking advantage of their photonic properties [2–9], which facilitates the detection of the target molecules using a microscope. Another example of the techniques related to LCs is drug delivery systems, where the drug molecule can have an LC property [10–12]. These techniques related to the LC system were developed mainly in LC-confined systems, i.e., systems where an LC is confined in a container. A molecular detection is realized by observing the structural change of the LC phase when it contacts the target molecule. In this case it is important to investigate the properties of the interface between the LC and the target material.

At the LC surface, the LC director, which corresponds to the local-averaged vector of the principal axes of LC molecules, is oriented to a certain direction with respect to the surface normal. Such a surface-orientation effect is called "anchoring." The anchoring is determined by surface conditions, which are, for example, given by the characteristics of the molecules that form the surface, the molecular arrangement, and the surface geometry. Due to the elasticity of the LC material, which has a much lower elasticity than usual solids (still typically 10 times larger than the thermal energy level), the surface ordering is propagated toward the bulk region of the LC, whose finite extension facilitates the detection of the target material. At a solid surface, the LC orientation is determined by the competition between the LC elasticity and the anchoring, where the interaction between the solid surface and the LC is one-directional, i.e., the solid surface affects the LC orientation, but the shape of the solid surface is not affected by the LC ordering [13].

On the other hand, when the interface is not rigid and can deform, the interfacial fluctuation is correlated to the director fluctuation of the LC at the interface. When an LC phase contacts an isotropic fluid, it is known that the interfacial tension is modified by the director fluctuation of the LC through the anchoring interaction [14].

An interesting behavior of a fluctuating interface that contacts an LC is observed when a molecular monolayer, such as a surfactant membrane, covers the interface. In this case, the coupling between the elasticity of the surfactant membrane and that of the LC leads to a rich variety of fascinating phenomena as will be discussed in this article.

Typical examples of surfactants are lipids and detergents, which stabilize the interface between hydrophilic (e.g., water) and hydrophobic (e.g., oil) materials by forming a membrane at the interface. Such a membrane shows elastic properties, e.g., the bending or curvature rigidity, which contributes to the shape change of the membrane [15]. When a hydrophobic LC is dissolved in a surfactant-water solution, the LC forms a domain separated from the water-rich phase by surfactant sheets. Due to the self-assembly of the surfactant molecules at the LC-water interface, the directional order of LC grows since the LC directors are oriented to a certain direction due to the steric or electric multipole interactions with the surfactant [16–18]. This effect is the anchoring effect mentioned above. Under the anchoring, an initial isotropic LC can change into an ordered state near the interface, which is known as the nematic wetting layer [19–21]. The nematic wetting layer can be formed even if the bulk region is in the isotropic phase at a temperature higher than the isotropic-nematic phase transition temperature. In the vicinity of a flexible interface, the nematic layer is expected to show different properties from those of the nematic layer near a rigid interface.

Rey [22] discussed a membrane that contacts a nematic LC and found that the property of the membrane fluctuation is altered according to the anchoring strength and the anchoring condition. Rey assumed that the free energy of the LC phase is given by the Frank elastic energy and considered the case with a weak and homeotropic anchoring condition (i.e., $|\boldsymbol{n} \cdot \boldsymbol{k}| = 1$ where $\boldsymbol{n}$ is the director of the LC and $\boldsymbol{k}$ is the membrane normal). Rey demonstrated that the inverse of the power spectrum of the membrane fluctuation is proportional to $(\gamma - W)q^2$, where γ is the interfacial tension, W is the anchoring modulus and is negative value for homeotropic

*softmatterlike@gmail.com

condition, and q is the magnitude of the wave vector $\boldsymbol{q} = (q_x, q_y)$ where the membrane is assumed to be parallel to the x-y plane on the average. In this case, the constraint $|\boldsymbol{n} \cdot \boldsymbol{k}| = 1$ and the assumption of a spatially uniform order parameter lead to a decreasing fluctuation of the membrane when the anchoring modulus W is increased. In the present article, although we will consider the case with a weak and homeotropic anchoring condition similar to Ref. [22], the above-mentioned constraints, i.e., $|\boldsymbol{n} \cdot \boldsymbol{k}| = 1$ and the spatially uniform order parameter, are not assumed. As a result, we will observe a different behavior in the properties of the membrane fluctuation compared to the system studied by Rey.

The outline of the present article is as follows: in Sec. II we will introduce our model for the LC layer confined by membranes using coarse-grained molecules, which will be simulated using the Monte Carlo method. In Sec. III we show the simulation results, and in Sec. IV we analyze our simulation results based on the Landau–de Gennes-type free energy that includes the effects of the anchoring at the interface. Finally, we summarize our results in Sec. V.

II. SIMULATION

A. Molecular model

For calculating the physical properties of a membrane that is in contact with an LC, we prepare a three-component system composed of an LC, surfactant, and water as follows: a layer composed of LC molecules with ellipsoidal shape is put between two surfactant monolayers which are placed parallel with each other, and an isotropic liquid composed of spherical molecules as a simplified model of water molecule is filled outside the two surfactant monolayers. All molecules are coarse-grained and are interacting through the following model potentials; the interactions between LC molecules are given by the Gay-Berne (GB) potential [23], which describes ellipsoidal particles. A surfactant molecule is composed of three spherical beads: one of them is named the "head particle" and attracts the water molecule, and the other two particles are named "tail particles" and repel the water. These particles are interacting with each other by the Lennard-Jones (LJ) potential and are connected by a harmonic spring potential to form a surfactant molecule. In addition, we assume that the surfactant molecule tends to take a straight molecular conformation by introducing a bending potential. Waterlike spherical molecules are interacting via a LJ potential that is the same as the potential exerted on particles composing the surfactants. On this system, we perform a Monte Carlo (MC) simulation with NPT ensemble. Although the dynamics of this system cannot be simulated with this MC simulation, we can obtain the equilibrium physical properties, such as interfacial tension and bending rigidity of the surfactant monolayer.

The GB potential describing the interactions between LC molecules has the form

$$\begin{aligned} U_{\mathrm{GB}}(\boldsymbol{r}_{ij}, \hat{\boldsymbol{u}}_i, \hat{\boldsymbol{u}}_j) = 4\epsilon_{ij}[\epsilon_1(\hat{\boldsymbol{u}}_i, \hat{\boldsymbol{u}}_j)]^{\mu}[\epsilon_2(\hat{\boldsymbol{r}}_{ij}, \hat{\boldsymbol{u}}_i, \hat{\boldsymbol{u}}_j)]^{\nu} \\ \times \{[\varrho_{ij}(\boldsymbol{r}_{ij}, \hat{\boldsymbol{u}}_i, \hat{\boldsymbol{u}}_j)]^{-12} \\ - [\varrho_{ij}(\boldsymbol{r}_{ij}, \hat{\boldsymbol{u}}_i, \hat{\boldsymbol{u}}_j)]^{-6}\}, \end{aligned} \tag{1}$$

where ϵ_{ij} is the interaction energy, $\boldsymbol{r}_{ij} = \boldsymbol{r}_i - \boldsymbol{r}_j$ is the relative position vector between i and j particles, and $\hat{\boldsymbol{u}}_i$ is the unit vector along the long axis of ith ellipsoidal particle. Using the distance between i and j particles $r_{ij} = |\boldsymbol{r}_{ij}|$, the relative position vector is given by $\boldsymbol{r}_{ij} = r_{ij}\hat{\boldsymbol{r}}_{ij}$, where $\hat{\boldsymbol{r}}_{ij}$ is the unit vector along the direction of $\boldsymbol{r}_{ij}$. The exponents μ and ν are the parameters used for adjusting the potential shape and are taken from Ref. [23]. In the GB potential, three functions, $\epsilon_1(\hat{\boldsymbol{u}}_i, \hat{\boldsymbol{u}}_j)$, $\epsilon_2(\hat{\boldsymbol{r}}_{ij}, \hat{\boldsymbol{u}}_i, \hat{\boldsymbol{u}}_j)$, and $\varrho_{ij}(\boldsymbol{r}_{ij}, \hat{\boldsymbol{u}}_i, \hat{\boldsymbol{u}}_j)$, appear. First, $\epsilon_1(\hat{\boldsymbol{u}}_i, \hat{\boldsymbol{u}}_j)$ is a measure of the magnitude of the interaction energy and is defined by the expression

$$\epsilon_1(\hat{\boldsymbol{u}}_i, \hat{\boldsymbol{u}}_j) = [1 - \chi^2(\hat{\boldsymbol{u}}_i \cdot \hat{\boldsymbol{u}}_j)^2]^{-1/2}, \tag{2}$$

where χ is defined as $\chi = (\kappa^2 - 1)/(\kappa^2 + 1)$ and $\kappa = \sigma_{\mathrm{e}}/\sigma_0$ is an aspect ratio of the ellipsoidal particle. σ_{e} and σ_0 in the expression of κ are a long axis length and short axis length, respectively, and σ_0 is chosen as the unit of the length scale of our simulation. Next, $\epsilon_2(\hat{\boldsymbol{r}}_{ij}, \hat{\boldsymbol{u}}_i, \hat{\boldsymbol{u}}_j)$ is a function of the angle between the long axes of i and j particles, $\hat{\boldsymbol{u}}_i$ and $\hat{\boldsymbol{u}}_j$, and the relative position vector $\hat{\boldsymbol{r}}_{ij}$ of the two ellipsoidal particles and is defined by

$$\epsilon_2(\hat{\boldsymbol{r}}_{ij}, \hat{\boldsymbol{u}}_i, \hat{\boldsymbol{u}}_j) = 1 - \chi'\left[\frac{(\hat{\boldsymbol{r}}_{ij} \cdot \hat{\boldsymbol{u}}_i)^2 + (\hat{\boldsymbol{r}}_{ij} \cdot \hat{\boldsymbol{u}}_j)^2 - 2\chi'(\hat{\boldsymbol{r}}_{ij} \cdot \hat{\boldsymbol{u}}_i)(\hat{\boldsymbol{r}}_{ij} \cdot \hat{\boldsymbol{u}}_j)(\hat{\boldsymbol{u}}_i \cdot \hat{\boldsymbol{u}}_j)}{1 - \chi'^2(\hat{\boldsymbol{u}}_i \cdot \hat{\boldsymbol{u}}_j)^2}\right], \tag{3}$$

where χ' is defined as $\chi' = (\kappa'^{1/\mu} - 1)/(\kappa'^{1/\mu} + 1)$ and $\kappa' = \epsilon_{\mathrm{ee}}/\epsilon_{\mathrm{ss}}$ is the interaction energy ratio between end-to-end (ϵ_{ee}) and side-by-side (ϵ_{ss}) configurations of two ellipsoidal particles (see Fig. 1). Finally, $\varrho_{ij}(\boldsymbol{r}_{ij}, \hat{\boldsymbol{u}}_i, \hat{\boldsymbol{u}}_j)$ is defined by

$$\varrho_{ij}(\boldsymbol{r}_{ij}, \hat{\boldsymbol{u}}_i, \hat{\boldsymbol{u}}_j) = \frac{r_{ij} - \sigma(\hat{\boldsymbol{r}}_{ij}, \hat{\boldsymbol{u}}_i, \hat{\boldsymbol{u}}_j) + \sigma_{ij}}{\sigma_{ij}}, \tag{4}$$

where $\sigma(\hat{\boldsymbol{r}}_{ij}, \hat{\boldsymbol{u}}_i, \hat{\boldsymbol{u}}_j)$ is defined as

$$\sigma(\hat{\boldsymbol{r}}_{ij}, \hat{\boldsymbol{u}}_i, \hat{\boldsymbol{u}}_j) = \sigma_{ij}\left\{1 - \chi\left[\frac{(\hat{\boldsymbol{r}}_{ij} \cdot \hat{\boldsymbol{u}}_i)^2 + (\hat{\boldsymbol{r}}_{ij} \cdot \hat{\boldsymbol{u}}_j)^2 - 2\chi(\hat{\boldsymbol{r}}_{ij} \cdot \hat{\boldsymbol{u}}_i)(\hat{\boldsymbol{r}}_{ij} \cdot \hat{\boldsymbol{u}}_j)(\hat{\boldsymbol{u}}_i \cdot \hat{\boldsymbol{u}}_j)}{1 - \chi^2(\hat{\boldsymbol{u}}_i \cdot \hat{\boldsymbol{u}}_j)^2}\right]\right\}^{-1/2}. \tag{5}$$

In this expression, σ_{ij} is the characteristic length scale of the excluded volume between i and j particles. The actual values of the four GB parameters (κ, κ', μ, ν) in Eq. (1), the energy unit ϵ_0, and the particle size unit σ_0 are given in Sec. II B.

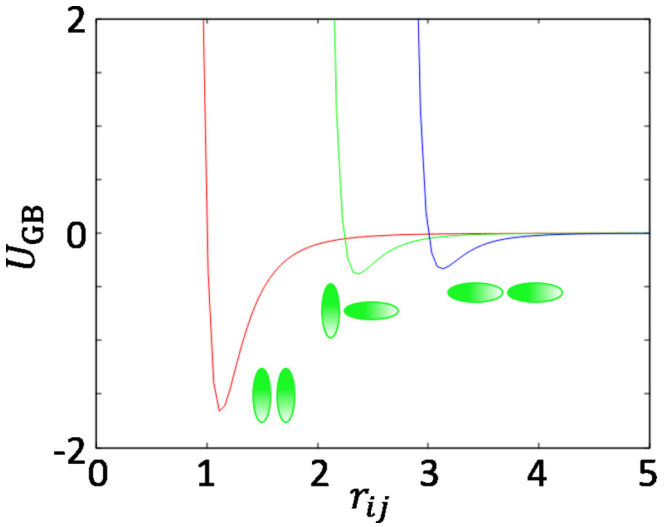

FIG. 1. Representative functional forms of the GB potential, where $(\kappa,\kappa',\mu,\nu) = (3.0, 5.0, 2.0, 1.0)$ are the same parameter set as used in our simulation. Schematic figures of two ellipsoids are the corresponding configurations for the respective forms of potential. The ratio of the energy depth of the side-by-side configuration (corresponding to the deepest energy depth, red line) to that of the end-to-end configuration (corresponding to the shallowest energy depth, blue line) shows the value of $\kappa' = 5.0$.

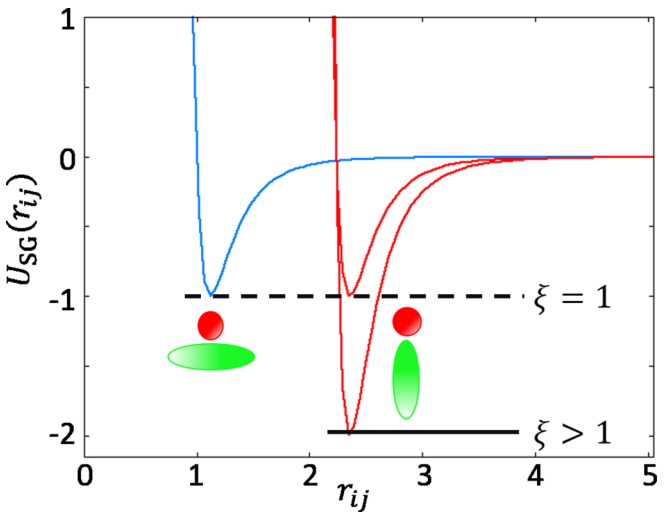

FIG. 2. Functional shapes of the potential U_{sg} for two representative configurations. One corresponds to the configuration with the short axis directed to the spherical particle, and the other corresponds to that with the long axis directed to the spherical particle, respectively. The potentials which contact the dotted line at the deepest point have the value $\xi = 1$, whereas the potential which contacts the solid line at the deepest point has $\xi > 1$.

The LJ potential describing the interactions between spherical particles is given by

$$U_{\rm LJ}(r_{ij}) = 4\epsilon_{ij}\left[\left(\frac{\sigma_{ij}}{r_{ij}}\right)^{12} - \left(\frac{\sigma_{ij}}{r_{ij}}\right)^{6}\right], \tag{6}$$

and the consecutive particles in a surfactant molecule are connected by a spring potential defined by

$$U_{\rm spring}(r_{ij}) = \tfrac{1}{2}k_{\rm spring}(r_{ij} - \sigma_{ij})^2, \tag{7}$$

where $k_{\rm spring}$ is the energy constant of the spring. A surfactant molecule, in addition, has the bending potential, which restricts its conformation and is defined by

$$U_{\rm bend}(\theta) = k_{\rm bend}[1 - \cos(\theta - \theta_0)], \tag{8}$$

where θ is the angle between the two consecutive bonds of the surfactant molecule, $k_{\rm bend}$ is the energy constant of the bending potential, and θ_0 is the stable angle between the two bonds composing the surfactant molecule. For simplicity, we assume that $\theta_0 = 0$, which means that our surfactant molecule is a coarse-grained molecule whose stable conformation is a straight one.

Here we introduce an important potential between ellipsoidal (labeled i) and spherical (labeled j) particles (the subscript "sg" means either spherical particle or GB particle) [24] as

$$U_{\rm sg}(\boldsymbol{r}_{ij},\hat{\boldsymbol{u}}_i) = 4\epsilon_{ij}[\epsilon_{\rm sg}(\hat{\boldsymbol{r}}_{ij},\hat{\boldsymbol{u}}_i)]^{\mu}\{[\varrho_{{\rm sg}ij}(\boldsymbol{r}_{ij},\hat{\boldsymbol{u}}_i)]^{-12} - [\varrho_{{\rm sg}ij}(\boldsymbol{r}_{ij},\hat{\boldsymbol{u}}_i)]^{-6}\}, \tag{9}$$

$$\varrho_{{\rm sg}ij}(\boldsymbol{r}_{ij},\hat{\boldsymbol{u}}_i) = \frac{r_{ij} - \sigma_{\rm sg}(\hat{\boldsymbol{r}}_{ij},\hat{\boldsymbol{u}}_i) + \sigma_{ij}}{\sigma_{ij}}, \tag{10}$$

$$\sigma_{\rm sg}(\hat{\boldsymbol{r}}_{ij},\hat{\boldsymbol{u}}_i) = \sigma_{ij}[1 - \chi(\hat{\boldsymbol{r}}_{ij}\cdot\hat{\boldsymbol{u}}_i)^2]^{-1/2}, \tag{11}$$

$$\epsilon_{\rm sg}(\hat{\boldsymbol{r}}_{ij},\hat{\boldsymbol{u}}_i) = 1 - \chi'_{\rm sg}(\hat{\boldsymbol{r}}_{ij}\cdot\hat{\boldsymbol{u}}_i)^2, \tag{12}$$

where $\chi'_{\rm sg} = 1 - \xi^{1/\mu}$ and $\xi = \epsilon_{\rm E}/\epsilon_{\rm S}$.

The parameter ξ is called the anchoring parameter herein and characterizes the anisotropy in the anchoring interaction. The parameter $\epsilon_{\rm E}$ corresponds to the interaction energy for the configuration where the long axis of the ellipsoidal particle is directed to the spherical particle, whereas $\epsilon_{\rm S}$ corresponds to that for the configuration where the short axis of the ellipsoidal particle is directed to the spherical particle. The representative shape of the potential is shown in Fig. 2. The parameter ξ is called the anchoring parameter herein and characterizes the anisotropic interaction. Then the anisotropic interaction potential $U_{\rm sg}$ includes the effect of the anchoring, whose strength changes depending on the direction of the ellipsoidal particle to the interacting spherical particle and is measured by the parameter ξ. As we will see, this anchoring parameter ξ plays an important role in the present work.

The interactions between different particles are either attractive or repulsive. In our work, the repulsive interaction is defined as the repulsive part of the nonbonded interaction potential. The particles are categorized into two groups: hydrophobic and hydrophilic. The ellipsoidal particles and the tail particles of the surfactants belong to the former, while the water particles and the head particles of the surfactants belong to the latter. Within the same group, the interactions are attractive, which is described by the nonbonded LJ potential defined in Eq. (6), while the interactions are repulsive between different groups where the repulsive part of the LJ potential is used. Due to these interactions, the LC layer can stably be maintained between two surfactant monolayers whose tails are directed to the LC, and the water region is outside of the surfactant monolayers.

B. Parameters and system setting

In this section, we give the values of the parameters used in our simulations. The interaction energy parameters ϵ_{ij} for all types of particle pairs are assumed to be the same value, i.e., $\epsilon_{00} = \epsilon_{11} = \epsilon_{22} = \epsilon_{33} = \epsilon_0$ and $\epsilon_{ij} = \sqrt{\epsilon_{ii}\epsilon_{jj}}$, where the subscripts $i = 0,1,2$, and 3 mean surfactant head, surfactant tail, isotropic water, and LC, respectively. ϵ_0 is the energy unit and is assumed to be equal to k_BT, where k_B is the Boltzmann constant and T is the temperature so that the dimensionless temperature is $T^* = k_BT/\epsilon_0 = 1.0$. The diameter of the spherical particles and the minor axis length of the ellipsoids are $\sigma_{00} = 1.05\sigma_0$, $\sigma_{11} = 1.0\sigma_0$, $\sigma_{22} = 1.0\sigma_0$, $\sigma_{33} = 1.0\sigma_0$, and $\sigma_{ij} = (\sigma_{ii} + \sigma_{jj})/2$, where σ_0 is the unit of length. The sizes of the surfactant head and tail are determined according to Ref. [25], where the surfactant model is more detailed than ours. The spring energy constant k_{spring} of the surfactant molecule is chosen as $100\epsilon_0/\sigma_0^2$, and the bending energy constant k_{bend} is $10\epsilon_0$ [25]. The characteristic parameters determining the form of ellipsoids are chosen as $(\kappa,\kappa',\mu,\nu) = (3.0,5.0,2.0,1.0)$, which were originally used in Ref. [23]. These molecular models are very simple models to interpret the change in the strength of the anchoring. Since our purpose is to understand the effects of the confined LC on the physical properties of the membrane qualitatively, a realistic model with realistic model parameters is not suitable.

We assume that the membranes are almost flat and introduce Cartesian coordinates (x,y,z) where the x-y plane is set parallel to the membrane and the z direction is the average normal direction of the membrane. In our MC simulations, the system evolves under the NPT ensemble, where the total number of the particles $N = 115\,200$ is composed of the number of the surfactants $N_s = 6400$, the LCs $N_l = 51\,200$, and the water $N_w = 44\,800$, and the dimensionless pressure is $P^* = P\sigma_0^3/\epsilon_0 = 3.0$. The temperature is $T^* = 1.0$ as has been explained before. These pressure and temperature values are chosen to realize the isotropic phase near the isotropic-nematic transition for the LC material (a phase diagram is given in Ref. [26]). The constant pressure condition is employed by exerting the constant stress with the same magnitude as P^* for all three directions so that the realized state is a stress-free state.

The MC simulations are performed as follows. First, we set an LC-confined surfactant membranes in the simulation box as an initial state and perform a simulation run for 1.0×10^5 Monte Carlo steps (MCSs) to obtain the energy minimum state. Then we perform other MC simulations for 1.0×10^5 MCS to obtain 500 snapshots from which we calculate the averaged values of the physical quantities.

C. Estimation of the interfacial properties

In order to estimate the physical properties of the membrane, we construct the free energy model of the membrane including such physical properties as the interfacial tension γ_{eff} and the bending rigidity K_{eff}, where the subscript "eff" means the effective quantities that include the influences not only from the membrane but also from the ellipsoidal molecules. We evaluate the mean square of the vertical displacement of the membrane in the Fourier space denoted as $h_{\boldsymbol{q}}$ [27], and fit the simulation data to a model interfacial free energy to obtain γ_{eff} and K_{eff}, where the model free energy of the membrane is given by

$$F = \int d\boldsymbol{a}\left\{\gamma_{\mathrm{eff}} + \frac{1}{2}K_{\mathrm{eff}}[\nabla_s \cdot \boldsymbol{m}(x,y)]^2\right\}. \tag{13}$$

Here $\boldsymbol{m} \approx [-\partial_x h(x,y), -\partial_y h(x,y), 1 - |\nabla_s h(x,y)|^2/2]$ is the membrane normal vector, $\boldsymbol{a}$ is the position vector on the membrane surface, and $d\boldsymbol{a} = \sqrt{1 + |\nabla_s h(x,y)|^2}\,dx\,dy$ is the area element, where $\nabla_s \equiv (\mathbf{1} - \boldsymbol{mm}) \cdot \nabla$ is the two-dimensional derivative operator on the membrane. Up to the second order in h, we can define $\nabla_s \approx (\mathbf{1} - \boldsymbol{e}_z\boldsymbol{e}_z) \cdot \nabla = (\partial_x, \partial_y, 0)$ where $\boldsymbol{e}_z$ is the basis vector in the z direction. Substituting these definitions into Eq. (13) and expanding it up to the second order in $|\nabla_s h(x,y)|$ and $|\nabla_s^2 h(x,y)|$, the free energy can be expressed in the Fourier space as

$$F = \frac{A_{\mathrm{m}}}{2N_{\mathrm{s}}^2}\sum_{\boldsymbol{q}}(\gamma_{\mathrm{eff}}\boldsymbol{q}^2 + K_{\mathrm{eff}}\boldsymbol{q}^4)|h_{\boldsymbol{q}}|^2, \tag{14}$$

where

$$h(x,y) = \frac{1}{N_{\mathrm{s}}}\sum_{\boldsymbol{q}} h(\boldsymbol{q})\exp(-i\boldsymbol{q}\cdot\boldsymbol{x}) \tag{15}$$

is the definition of the Fourier component $h_{\boldsymbol{q}}$, A_{m} is the total area of the membrane, and $\boldsymbol{x} = (x,y)$. The symbol N_{s} in the denominator in Eq. (15) is used as the normalization factor instead of the usual number of mesh points. Assuming a canonical ensemble, the mean squared displacement of the membrane position $\langle|h_{\boldsymbol{q}}|^2\rangle$ is obtained as

$$\langle|h_{\boldsymbol{q}}|^2\rangle = \frac{N_{\mathrm{s}}^2 k_{\mathrm{B}}T}{A_{\mathrm{m}}(\gamma_{\mathrm{eff}}q^2 + K_{\mathrm{eff}}q^4)}, \tag{16}$$

where $q = |\boldsymbol{q}|$. First, we calculate $h_{\boldsymbol{q}}$ from the molecular simulation by defining the local $h(x,y)$ as $h(x,y) = \sum_i h(x_i,y_i)\delta(x-x_i)\delta(y-y_i)/[\sum_{i'}\delta(x-x_{i'})\delta(y-y_{i'})]$ where $(x_i,y_i,z_i) = (x_i,y_i,h(x_i,y_i))$ corresponds to the centers of mass of ith surfactant molecule. Here we assume the incompressibility condition that means $\sum_i \delta(x-x_i)\delta(y-y_i) = N_{\mathrm{s}}/A_{\mathrm{m}}$ on the surfactant membrane. Second, by fitting the simulation data with Eq. (16) on double logarithmic scales, one can obtain the effective interfacial tension γ_{eff} and the effective bending rigidity K_{eff} as the coefficients of second- and fourth-order terms in $\boldsymbol{q}$.

III. SIMULATION RESULTS

In our simulations, the most important parameter is the anchoring parameter ξ, which is a measure of the anisotropic interaction between the tail of the surfactant and the LC molecule (see Fig. 2). We change the value of ξ while the isotropic interaction parameter ϵ_0 is fixed. When ξ is increased, the attractive interaction energy between the LC molecules and the surfactant molecules is also increased. In our simulation, the number of the LC particles penetrating into the membrane is fewer than that of the LC particles contacting the membrane. Then increasing ξ leads to a change in the size and shape of the simulation box because the pressure in the x-y plane becomes smaller than that in the z direction due to the increase in the attractive interaction. Therefore, the size of the simulation box in the z direction becomes smaller and that in the x and y

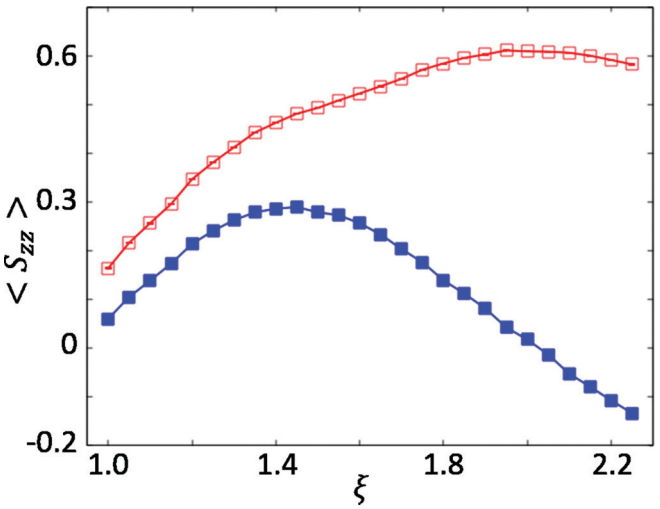

FIG. 3. The red line shows the change in the maximum value of the LC scalar order parameter in the LC layer $S_{\max}$ as a function of the anchoring parameter ξ. The blue line shows the change in the order parameter just at the interfacial position S_{int}.

FIG. 4. Snapshot pictures of the LC molecules near the interface for (a) $\xi = 1.0$, (b) $\xi = 1.4$, and (c) $\xi = 1.8$.

direction becomes larger. At the same time, the LC molecules near the interface orient to the z direction on average due to the anchoring interaction and the LC order parameter increases. In this case, however, the density of the LC confined by the membranes is kept constant.

In order to characterize the orientation order of LC, we introduce the LC order parameter S, which is defined as the largest eigenvalue of the tensor order parameter $\boldsymbol{Q}$ defined as

$$\boldsymbol{Q} = \left\langle \boldsymbol{uu} - \tfrac{1}{3} \right\rangle, \tag{17}$$

where $\boldsymbol{u}$ is the local molecular director vector of the LC. To investigate the change of S in the z direction, we calculate the local average of S in each layer parallel to the xy plane with a thickness σ_0.

Figure 3 shows the maximum value of the LC order parameter in the membrane normal direction $S_{\max}$ (red line) and the value of the LC order parameter at the interface position S_{int} (blue line), respectively. Here $S_{\max}$ is defined as the maximum value of the profile of the order parameter of the LC in the z direction, which is measured near the membrane (i.e., within the region where the order parameter S is affected by the interface), and S_{int} is measured at the point where the LC density profile takes a half value of its bulk LC density (i.e., the centers of mass of the LC molecules that contribute to S_{int} are just at the interfacial position). As one can see, $S_{\max}$ is monotonically increasing as ξ increases, while S_{int} shows the maximum at $\xi \approx 1.4$.

These behaviors can be confirmed by the snapshot of the LC molecules near the membrane in the equilibrium state (see Fig. 4 where membranes are not shown). From these snapshots, we observe that the number of horizontally directed LC molecules in the vicinity of the membrane is increased as ξ is increased. This corresponds to the change in the behavior of S_{int}. We can also observe that the orientation of the LC molecules near the interface [see the LC molecules near the interface in Figs. 4(a)–4(c)] is more directed to the interfacial normal as confirmed from the behavior of $S_{\max}$. Although $S_{\max}$ is an increasing function of the anchoring parameter ξ, S_{int} shows a nonmonotonic behavior, which we attribute to the membrane fluctuation, as will be discussed below.

The above behaviors of the two types of order parameters $S_{\max}$ and S_{int} can also be confirmed by evaluating the orientation distribution function of LC molecules shown in Fig. 5. This $P(\theta)$ is proportional to the population of LC molecules with molecular direction θ that have an overlap with the average position of the membrane. In Fig. 5 the distribution function $P(\theta)$ is normalized by the Jacobian of the spherical coordinate $\sin\theta$.

From Fig. 5 we can recognize several characteristics of $P(\theta)$. First, even if $\xi = 1$ (i.e., isotropic anchoring), the probability distribution $P(\theta)/\sin\theta$ is not uniform. This is due to the fact that the directors of LC molecules near the membrane are affected not only by the anchoring interaction but also by the excluded volume interaction which attributes to loss of the translation entropy of the LC molecules near the interface. As a result of the competition between these two interactions, the director of the LC molecules avoids aligning in the membrane normal direction, which is shown

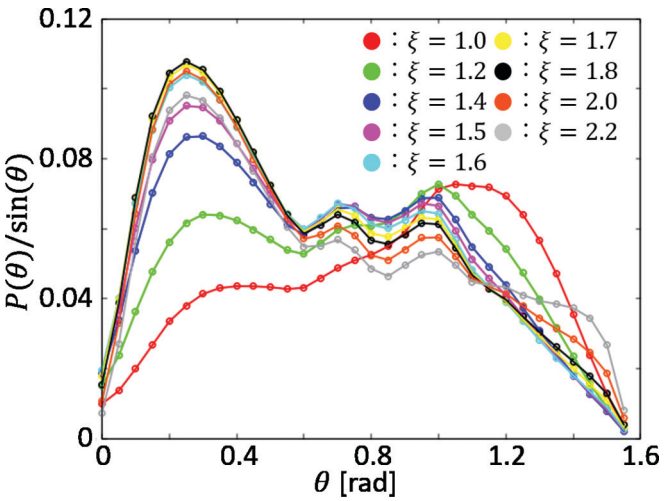

FIG. 5. The distribution function of the angle between the LC director and z axis, which is defined as $\arccos(\boldsymbol{n}_z)$ just at the interface. The distribution function is normalized by the Jacobian of the spherical coordinate system $\sin\theta$. The correspondence between color and anchoring parameter ξ is shown.

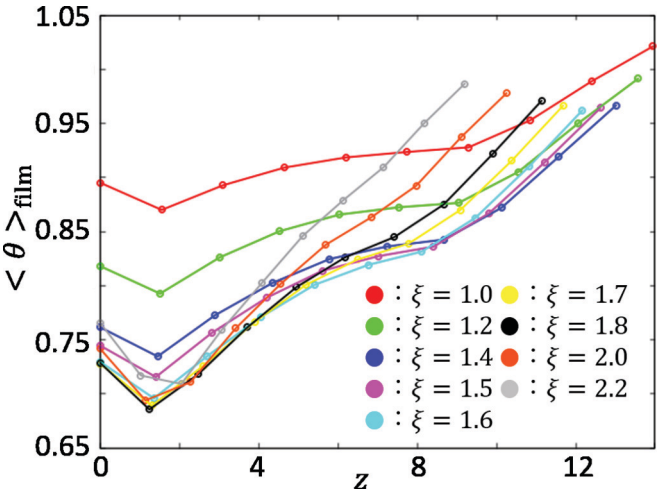

FIG. 6. The dependence of average $\theta(z)$ on the z direction, which is estimated in each thin films with the thickness σ_0. The correspondence between color and anchoring parameter ξ is shown.

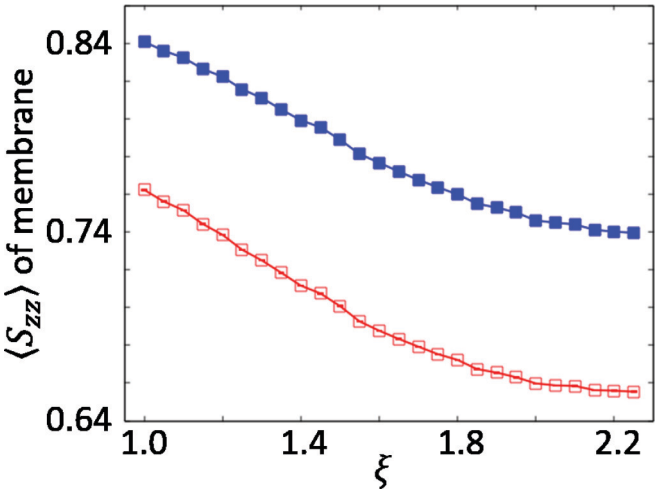

FIG. 7. The red line shows the change in the director order parameter of the surfactant molecule defined by the direction of the hydrophobic tails S_{tt}, and the blue line shows the order parameter defined as the end-to-end vector S_{ee} of the surfactant molecule, both shown as functions of the anchoring strength ξ.

by the dip in $P(\theta)/\sin\theta$ around $\theta = 0$. Second, when the anchoring parameter ξ is increased, $P(\theta)/\sin\theta$ in the small θ region ($\theta < 0.6$) increases to $\xi = 1.8$ and forms a peak around $\theta = 0.3$, which is a sign of oblique alignment as a result of the competition between the anchoring and excluded volume interactions mentioned above. At the same time, $P(\theta)/\sin\theta$ in the large θ region ($1.0 < \theta$) decreases in order to compensate for the growth in the smaller θ region. Third, the region at $\theta > 1.2$ initially decreases up to $\xi < 1.8$, and then this region starts to increase for $\xi > 1.8$. These behaviors are the evidence of the appearance of the peak in the interfacial orientation parameter $S_{\rm int}$. Although the excluded volume effect on the behavior of the angular distribution function is strong enough, as mentioned above, the very small distribution $P(\theta)/\sin\theta|_{\theta=\pi/2} \sim 0$ is due to the ellipsoidal shape of the LC molecules: As the LC molecules with $\theta = \pi/2$ have a larger projection area onto the membrane, they interact with the membrane with a larger repulsive interaction than those of the LC molecules with $\theta = 0$ when they approach the membrane. As a result, the population of LC molecules with $\theta = \pi/2$ just at the membrane decreases.

As shown in Fig. 6, we can observe the dependence of average $\langle\theta(z)\rangle_{\rm film}$ on the distance from the membrane (i.e., z coordinate of the LC molecules), which gives more information on the difference between $S_{\rm max}$ and $S_{\rm int}$. The value of $\langle\theta(z)\rangle_{\rm film}$ near the membrane is almost monotonically decreasing as ξ is increased. This means that the LC directors are more and more pointed in the membrane normal direction due to the homeotropic anchoring ($\xi > 1$). In addition to such a homeotropic anchoring tendency, we can also observe a small peak at $z = 0$ (i.e., at the membrane). This peak corresponds to the existence of planar alignment of LC molecules at the membrane, which is consistent with our observation from Fig. 4. This planar alignment is the origin of the difference in the behaviors of $S_{\rm max}$ and $S_{\rm int}$.

Similar order parameters of the molecular orientation can be defined for the surfactant molecules. Figure 7 shows the order parameter of the surfactant directors. The red curve shows the order parameter $S_{\rm tt}$ (order parameter of the tail part of the surfactant molecule), which is defined as the averaged value of the director which points from one tail particle to the other in a single surfactant molecule, and the blue curve shows order parameter $S_{\rm ee}$ (order parameter of end-to-end director of the whole surfactant molecule), which is defined as the averaged value of the director which points from the end tail particle to the head particle in a single surfactant molecule. From this figure, we can confirm that these two order parameters show the same behavior, while the LC order parameters (Fig. 3) show different behavior from those of $S_{\rm tt}$ or $S_{\rm ee}$. Therefore, the behavior of the LC orientation does not directly follow the behavior of the director of the surfactant molecules through the anchoring. Note that an effective steric interaction between the LC director and the surfactant director exists, besides the anchoring interaction defined using ξ. Although the interaction between the LC and the membrane is purely isotropic for $\xi = 1$, there exists an anisotropic interaction originating from the steric interaction between the LC molecule and the surfactant molecule, which induces the order of the LC at $\xi = 1$; see Fig. 3. The LC order parameter S at $\xi = 1$ is very small ($S_{\rm max} \sim 0.16$ and $S_{\rm int} \sim 0.06$) but finite. Then we can recognize that the LC ordered state exists.

Next we will see the change in the physical properties of the membrane according to the change in ξ. The membrane properties, such as the interfacial tension $\gamma_{\rm eff}$ and the bending rigidity $K_{\rm eff}$, are plotted as functions of the anchoring parameter ξ in Figs. 8 and 9, respectively.

The decreasing of $\gamma_{\rm eff}$ (Fig. 8) with increasing ξ is interpreted as follows. Increasing the value of ξ, the depth of the interaction potential between LC molecule and the hydrophobic particle of the surfactant is increased depending on their configuration with respect to the LC orientation (see Fig. 2). The depth of the potential which corresponds to the configuration of the LC long axis directed to the spherical particle is deeper than that which corresponds to the configuration of the LC short axis directed to the spherical particle. In this case, the projection area of the membrane onto

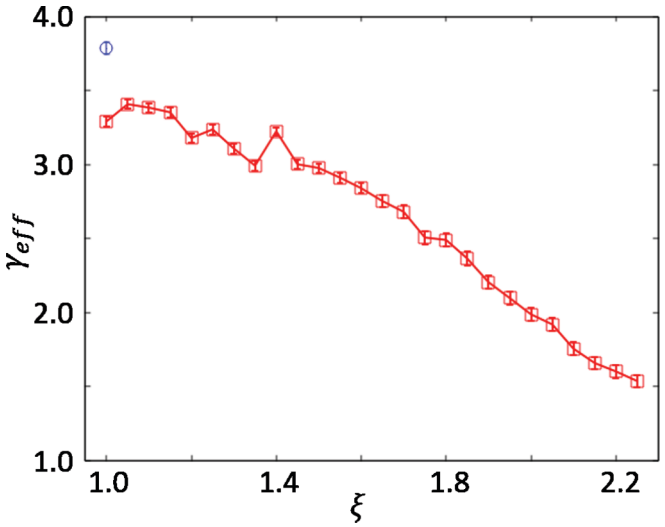

FIG. 8. The red line shows the interfacial tension of the membrane $\gamma_{\rm eff}$ as a function of the anchoring strength ξ. The blue data at $\xi = 1$ show the interfacial tension γ_0 for the case with the oil-confined system where the LC molecules are replaced by spherical hydrophobic particles (the interaction energy between oil and surfactant tails is $\epsilon_0 = 1$).

the x-y plane is expanded as mentioned above. The larger the membrane area is, the softer the membrane with respect to its area expansion becomes, because the membrane with larger area behaves as obtaining a more expanded area. Then $\gamma_{\rm eff}$ decreases when ξ increases. Such a decrease in the interfacial tension is observed not only in the LC-confined system but also in an oil layer confined by membranes, for example. In the LC system, the influence from the fluctuation of the LC orientation appears. When ξ increases, the fluctuation of the interaction energy between the LC and the membrane through the anchoring originating from the thermal fluctuation of the LC orientation also increases (see Fig. 2). When ξ increases,

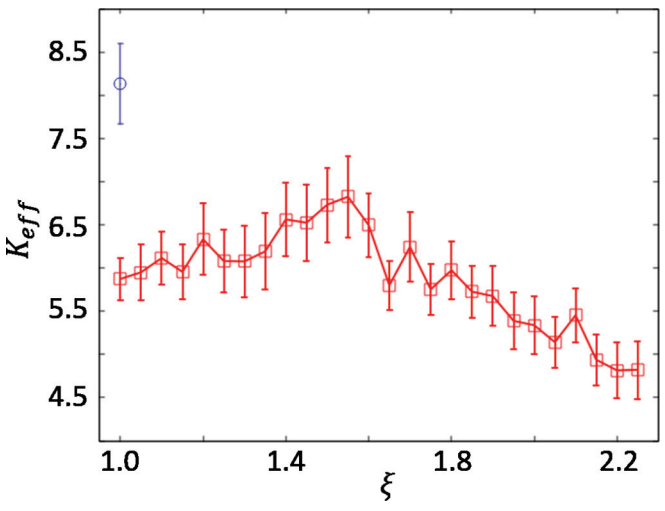

FIG. 9. The red line shows the bending rigidity of the membrane $K_{\rm eff}$ as a function of the anchoring parameter strength ξ. The blue data at $\xi = 1$ show the bending rigidity K_0 in the oil-confined system (the interaction energy between oil and surfactant tails is $\epsilon_0 = 1$).

the change in the interaction energy becomes larger with respect to the change in the LC orientation. The larger the fluctuation of the interaction energy, the larger the fluctuation of the area of the membrane becomes since the membrane area is determined by the LC-surfactant interaction. In this case, since the membrane becomes softer with respect to the expansion of the area, $\gamma_{\rm eff}$ also decreases. The nematic order at the interface strengthens the effect of the orientational fluctuation for the interfacial tension $\gamma_{\rm eff}$. If the LC is in the isotropic phase at the interface, the fluctuation of the local interaction energy between the surfactants and the LCs is small irrespective of the interfacial shape because the interface does not affect the distribution of the molecular axis vectors of the LC. In this case, $\gamma_{\rm eff}$ is unchanged.

Note that the decreasing of the interfacial tension is different from the analytical result by Rey [22] because the orientational order in our case can fluctuate, while that in the system discussed in Ref. [22] cannot fluctuate.

When $\xi > 1$, in our case, the LC orientation averaged over the interfacial region is directed to the averaged interfacial normal direction due to the anchoring (see Fig. 3). Such an orientation direction does not in general coincide with the natural direction of the LC determined by its elasticity. Then the local LC directions near the interface are determined by the competition between the contribution from the LC elasticity and that from the anchoring, which leads to a renormalization of the effective bending rigidity. Such a competition leads to two different regimes in the anchoring strength divided at a certain threshold value $\xi = \xi_{\rm m}$, which will be interpreted later.

The bending rigidity $K_{\rm eff}$ in Fig. 9 shows a nonmonotonic behavior as a function of the anchoring parameter ξ. With increasing ξ, first $K_{\rm eff}$ slightly increases and then decreases across a certain value of $\xi = \xi_{\rm m}$. When the anchoring effect is small compared to the LC elasticity, i.e., $1 < \xi < \xi_{\rm m}$, the local LC director near the interface does not fit to the local membrane normal due to the LC elasticity, which avoids a spatial variation of the LC directors. Then most of the LC directors are oriented to the same direction, i.e., the *average* normal direction of the membrane, resulting in the development of the nematic layer. In this case, when the membrane fluctuates, the mismatch between the local membrane normal and the LC director imposes a penalty for the anchoring interaction, resulting in an increase in the effective bending rigidity.

Contrary to the above weak anchoring case, the behavior changes when $\xi > \xi_{\rm m}$, i.e., a strong anchoring case. In this case, the bending rigidity changes its dependence on ξ from increasing to decreasing behaviors. If the effect of the homeotropic anchoring is strong enough, the local LC directors near the membrane tend to orient to the local membrane normal. Then the LC orientation near the interface is distorted when the membrane fluctuates, which leads to an increase in the penalty due to the LC elasticity. To suppress this elastic penalty of LC, the LC molecules just at the interface, where the LC molecules have a contact with the surfactant on the membrane, change direction from the average membrane normal into the lateral direction along the membrane. In this case, when the membrane fluctuates in the direction perpendicular to the LC orientation in the lateral plane, the LC elastic penalty is not imposed, and the bending rigidity of the membrane effectively decreases. Such a change in the LC

orientation from the membrane normal to the lateral direction of the membrane is realized by the so-called depletion effect, which originates from the entropic effect with respect to the steric hindrance on the translation of the LC molecules just at the interface (similar behavior is confirmed in the LC-confined system in Ref. [13] where the interface is not flexible but rigid.). The change in the LC orientation just at the interface is confirmed by the orientation order parameter of the LC near the membrane, which shows a similar behavior to the bending rigidity (see $S_{\rm int}$ in Fig. 3); that is, the order changes its tendency from increasing to decreasing behavior. Note that the LC molecules slightly away from the membrane (i.e., LC molecules whose centers of mass locate within $2\sigma_0$ from the membrane position) are directed to the membrane normal (i.e., smaller value of θ), which is due to the homeotropic anchoring condition for $\xi > 1$ (see Fig. 6). Then the effect of the anchoring remains so as to minimize the total interaction energy although the LC orientations are mixed (both z and x-y orientations exist) near the interface.

The orientational behavior of the LC discussed above can be realized due to the weak nematic in the bulk region. If the bulk LC is in the nematic phase, the membrane fluctuation can be transferred into the bulk region, resulting in a higher penalty from the LC elasticity than that in our case.

At the end of this section, we briefly discuss the case of planar anchoring with $\xi < 1$. Such a planar anchoring can be realized by using $\xi < 1$ and larger ϵ_0. However, in the present study, we excluded such a planar anchoring case partly because the range of ξ for the planar anchoring ($0 < \xi < 1$) is very narrow compared with that for the homeotropic anchoring ($1 < \xi$), and partly because the planar anchoring for $\xi \to 0$ requires an increasingly large value of ϵ_0, which is not consistent with our treatment for the homeotropic anchoring case where ϵ_0 is kept constant.

IV. COARSE-GRAINED FREE ENERGY MODEL (CONTINUUM MODEL) AND ITS MINIMIZATION

In this section, by using an appropriate simple free energy model, we try to explain why the interfacial properties change with ξ as was discussed in the previous section.

First, we propose a coarse-grained free energy model for our simulation system. We choose a tensor order parameter of the LC, $Q_{\alpha\beta}(\boldsymbol{r})$, and an interfacial normal vector $m_\alpha(x,y)$ ($\alpha = x,y,z$) is selected as the order parameters for our model-free energy. We neglect the contribution from the isotropic liquid that fills the region outside the membrane. In this free energy, the reference state is taken as the isotropic phase of the LC and the planar shape of the membrane. Then the general form of the free energy is written as

$$F = \int_0^{L_x}\int_0^{L_y}\int_{-z_0}^{z_0} d\boldsymbol{r}\left\{\frac{A}{2}Q_{\alpha\beta}Q_{\alpha\beta} + \frac{L}{2}\partial_\alpha Q_{\beta\gamma}\partial_\alpha Q_{\beta\gamma}\right\} + \int_0^{L_x}\int_0^{L_y} d\boldsymbol{a}\left\{\gamma_0 + \frac{K_0}{2}(\partial_\alpha m_\alpha)^2 + \frac{\gamma_{\rm f}}{2}m_\alpha Q_{\alpha\beta}m_\beta + K_1 m_\alpha \partial_\beta m_\gamma \partial_\alpha Q_{\beta\gamma} + \frac{K_{\rm b}}{4}m_\alpha Q_{\alpha\beta}m_\beta(\partial_\gamma m_\gamma)^2\right\}\Big|_{\pm z_0}. \quad (18)$$

In this expression, A and L are the coefficients of the bulk isotropic LC, where the one constant approximation is adopted to the coefficient L of the Landau-de Gennes free energy [1], and γ_0 and K_0 are the interfacial tension and bending rigidity of the membrane as expressed in Sec. II C, and $z = \pm z_0$ are the average positions of the membranes in the z direction. $\gamma_{\rm f}$ corresponds to the anchoring of LC to the membrane normal, which is negative because of the homeotropic anchoring condition in our simulation, and K_1 is the coupling constant between the LC elasticity and the membrane elasticity. Both of these parameters $\gamma_{\rm f}$ and K_1 are assumed to depend on ξ. Since $K_{\rm b}$ term expresses the elastic rigidity of the ordered LC near the interface, $K_{\rm b}$ is assumed to be independent of ξ. As a result, we assume that only $\gamma_{\rm f}$ and K_1 depend on ξ, and therefore the contribution from the anchoring comes into the analysis only through these parameters.

The tensor order parameter $Q_{\alpha\beta}(\boldsymbol{r})$ is defined in Eq. (17). In our simulation, since the bulk LC is in the weak nematic phase, $Q_{\alpha\beta} \approx S(\boldsymbol{r})[n_\alpha n_\beta - (1/3)\delta_{\alpha\beta}]$ is small, where n_α is the α component of the local main axis, and $S(\boldsymbol{r})$ is the local scalar order parameter of LC. However, in the vicinity of the membrane, it is expected that $Q_{\alpha\beta} \approx S(\boldsymbol{r})[m_\alpha m_\beta - (1/3)\delta_{\alpha\beta}]$ due to the anchoring. Thus we write $Q_{\alpha\beta}(\boldsymbol{r})$ in two different forms as

$$\boldsymbol{Q}(-z_0 < z < z_0) = \tfrac{3}{2}S(\boldsymbol{r})\big[\boldsymbol{n}(\boldsymbol{r})\boldsymbol{n}(\boldsymbol{r}) - \tfrac{1}{3}\big], \quad (19)$$

$$\boldsymbol{Q}(z = \pm z_0) = \tfrac{3}{2}S(\boldsymbol{r})\big[\boldsymbol{m}(\boldsymbol{r})\boldsymbol{m}(\boldsymbol{r}) - \tfrac{1}{3}\big]. \quad (20)$$

In these expressions, $S(\boldsymbol{r})$, n_α, and m_α are the local averaged values. Since the membrane is planar on the average, m_α is written as

$$\boldsymbol{m}(x,y) = \big(-\partial_x h(x,y), -\partial_y h(x,y), 1 - \tfrac{1}{2}|\nabla h(x,y)|^2\big), \quad (21)$$

where $h(x,y)$ represents the displacement of the membrane in the z direction from the average position. Using these expressions of the order parameters, and using the assumption of the small deformation of the membrane, i.e., $|\nabla h| \ll 1$, and $d\boldsymbol{a} = \sqrt{1+|\nabla h|^2}\,dx\,dy \approx (1+|\nabla h|^2/2)\,dx\,dy$, the free energy is rewritten as

$$\begin{aligned} F = {} & \frac{3}{4}\int d\boldsymbol{r}\{AS(\boldsymbol{r})^2 + L|\nabla S(\boldsymbol{r})|^2\} \\ & + \int dx\,dy\left\{\frac{\gamma_0}{2}|\nabla_s h(x,y)|^2 + \frac{K_0}{2}\big[\nabla_s^2 h(x,y)\big]^2\right. \\ & + \frac{\gamma_{\rm f}}{2}[S(x,y,z_0) + S(x,y,-z_0)]\left[1 + \frac{1}{2}|\nabla_s h(x,y)|^2\right] \\ & + \frac{K_1}{2}[\partial_z S(x,y,z_0) + \partial_z S(x,y,-z_0)]\nabla_s^2 h(x,y) \\ & \left. + \frac{K_{\rm b}}{4}[S(x,y,z_0) + S(x,y,-z_0)]\big[\nabla_s^2 h(x,y)\big]^2\right\}, \end{aligned} \quad (22)$$

where the constant term is omitted. In Eq. (22) the contribution from the elasticity of the LC directors in the bulk region is neglected due to weak nematic state, and we also assumed that the membrane properties are the same for the two membranes at $z = \pm z_0$. The third-order term (the $\gamma_{\rm f}$ term) is included

because it gives an important contribution to the interfacial tension as will be shown below.

This free energy model is Fourier transformed by considering the Fourier components of the order parameters in the horizontal plane (x,y) as

$$S(\boldsymbol{r}) = \frac{1}{N_{\rm LC}} \sum_{\boldsymbol{q}} S(\boldsymbol{q},z) \exp(-i\boldsymbol{q}\cdot\boldsymbol{x}), \tag{23}$$

$$h(x,y) = \frac{1}{N_{\rm s}} \sum_{\boldsymbol{q}} h(\boldsymbol{q}) \exp(-i\boldsymbol{q}\cdot\boldsymbol{x}), \tag{24}$$

where $N_{\rm LC}$ and $N_{\rm s}$ are the numbers of LC and surfactant molecules, respectively, and $\boldsymbol{x}$ and $\boldsymbol{q}$ are the position vector in the (x,y) plane and the wave vector in the Fourier space, respectively. Substituting these Fourier transformed expressions into Eq. (22), minimizing the result with respect to $S(\boldsymbol{q},z)$, and solving the differential equation with respect to z, we obtain the modified coefficients of $S(\boldsymbol{q},z)$. Consequently, we can rewrite the free energy up to the second order in the Fourier components of the membrane height $h(\boldsymbol{q})$ as

$$F = \frac{L_x L_y}{N_{\rm s}^2} \sum_{\boldsymbol{q}} \left[\left(\gamma_0 - \frac{\gamma_{\rm f}^2}{\gamma_{\rm LC}} \right) \boldsymbol{q}^2 + \left(K_0 - \frac{K_1^2}{E_{\rm LC}} - \frac{\gamma_{\rm f} K_{\rm b}}{\gamma_{\rm LC}} \right) \boldsymbol{q}^4 \right] |h_{\boldsymbol{q}}|^2, \tag{25}$$

where $E_{\rm LC} = L l_{\rm LC}$ and $\gamma_{\rm LC} = L/l_{\rm LC}$ are the scale of the energy and the interfacial tension expressed in terms of the LC parameters, respectively, and $l_{\rm LC} = \sqrt{L/A}$ is the characteristic length scale of the LC. Here we took the limit $z_0 \to \infty$ by assuming the weak correlation between two membranes via the confining LC due to the weak nematic phase in the bulk region. As one can see, the effective interfacial tension and the effective bending rigidity in Eq. (25) are given by

$$\gamma_{\rm eff} = \gamma_0 - \frac{\gamma_{\rm f}^2}{\gamma_{\rm LC}}, \tag{26}$$

$$K_{\rm eff} = K_0 - \frac{K_1^2}{E_{\rm LC}} - \frac{\gamma_{\rm f} K_{\rm b}}{\gamma_{\rm LC}}, \tag{27}$$

in terms of the coupling constants $\gamma_{\rm f}$, K_1, and $K_{\rm b}$.

Next we give the detailed expressions of $\gamma_{\rm f}$, K_1, and $K_{\rm b}$ as functions of ξ. As was mentioned in Eq. (18), we assume that $\gamma_{\rm f}$ and K_1 depend on ξ, but $K_{\rm b}$ is independent of ξ. First, since $\gamma_{\rm f}$ expresses the orientational anchoring effect and corresponds to the homeotropic condition for $\xi > 1$ in our simulation [$\xi = 1$ gives no anchoring because $\chi'_{\rm sg} = 0$; see Eq. (12)], we assume $\gamma_{\rm f} \approx a(1-\xi)$, where a is a constant independent of ξ. Second, K_1 expresses the effect of the coupling between the LC orientation and the membrane fluctuation. In our simulation, the LC molecules which contact the surfactants at the interface tend to be parallel to the x-y direction for $\xi > \xi_{\rm m}$. This is because the penalty from the LC elasticity increases due to the membrane fluctuation when the LC molecules orient to the membrane normal (so the homeotropic condition is disrupted at the interface where the LC and the surfactant contact each other, but it remains slightly far away from the membrane as mentioned in Sec. III). Then the coupling becomes stronger for $\xi > \xi_{\rm m}$. Assuming that $K_1 \approx d_{\rm a}(1-\xi)$ where $d_{\rm a}$ is a ξ-independent constant, the exchange of the contribution from the LC elasticity to the anchoring can be expressed in Eq. (27).

Then Eqs. (26) and (27) are rewritten as

$$\gamma_{\rm eff} = \gamma_0 - \frac{a^2}{\gamma_{\rm LC}}(1-\xi)^2, \tag{28}$$

$$K_{\rm eff} = K_0 - \frac{d_{\rm a}^2}{E_{\rm LC}}(1-\xi)^2 - \frac{a}{\gamma_{\rm LC}} K_{\rm b}(1-\xi). \tag{29}$$

Fitting these expressions to our simulation data, we get

$$a = 0.47 \pm 0.069, \tag{30}$$

$$d_{\rm a} = 0.89 \pm 0.063, \tag{31}$$

$$K_{\rm b} = 0.71 \pm 0.16, \tag{32}$$

$$\xi_{\rm m} = 1.4 \pm 0.11. \tag{33}$$

The qualitative behavior of the simulation data can be reproduced by Eqs. (28) though there are still deviations in the detail (see Fig. 10). Here we expect that the inconsistency is caused by the difference between the microscopic description in the molecular simulation and the macroscopic description in the continuum field model. The interfacial tension and the bending rigidity estimated from the molecular simulation are under the influence of the interaction between the ordered states in the LC and the membrane as well as under the influence by the interaction between the LC molecules and the surfactant molecules. The continuum field model takes into account only the former effect because of its coarse-grained nature. This is the origin of the relatively large deviation between the molecular simulation result and the result of the continuum field model. However, we believe that our continuum model can at least reproduce the qualitative behavior of the system.

From these results of fitting, we understand that (1) the decreasing behavior of the effective interfacial tension is due to the fluctuation of the orientation order strengthened by the anchoring effect, (2) the increasing behavior of the effective bending rigidity in $1 < \xi < \xi_{\rm m}$ is due to the effect of the nematic layer of the LC, and (3) the decreasing behavior of the effective bending rigidity in $\xi_{\rm m} < \xi$ is due to the coupling between the fluctuation of the LC and the fluctuation of the membrane shape.

Here we discuss the origin of the increase in the number of LC molecules aligned in the parallel direction to the membrane just at the membrane position, which is shown by the small peak in the orientation order parameter $S(z)$ around $z = 0$ in Fig. 6. Due to the K_1 term in the free energy Eq. (22), it is understood that, when $K_1 < 0$, $\partial_z S(x,y,\pm z_0) > 0$ for $\nabla_s^2 h(x,y) > 0$ (the membrane is concave towards the water phase) and $\partial_z S(x,y,\pm z_0) < 0$ for $\nabla_s^2 h(x,y) < 0$ (the membrane is convex towards the water phase) are preferred, respectively. Therefore, the negative slope of $S(z)$ associated with the peak near the membrane in Fig. 6 can be explained as a result of the convex shape of the membrane towards the water phase. In this case, in order to fill the space between the membrane and the LC phase, planar alignment of LC molecules is generated as was observed in Fig. 4. This tendency is of course reduced by the excluded volume interaction between the LC molecule and the membrane that has a finite molecular volume.

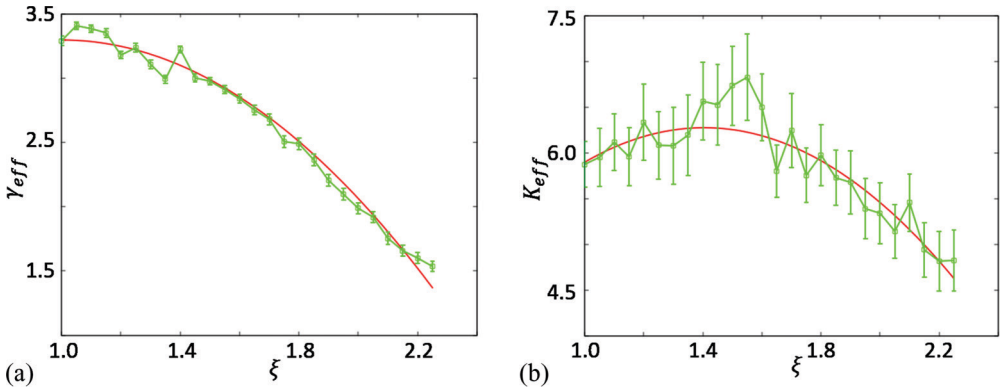

FIG. 10. Fittings for $\gamma_{\rm eff}$ and $K_{\rm eff}$. The green data are both the results of our simulation. The red smooth curves are the fitting function.

V. CONCLUSION

In this article, we estimated the mechanical properties of a membrane that is affected by the contact with a low molecular weight LC. By performing MC simulations, we found that the interfacial tension of the membrane is decreased by increasing the strength of the homeotropic anchoring, and the bending rigidity $K_{\rm eff}$ shows a nonmonotonic behavior as a function of the anchoring strength ξ. When ξ is increased, $K_{\rm eff}$ first increases due to the increase in the rigidity of the ordered LC near the interface. Then, for $\xi > \xi_{\rm m}$, $K_{\rm eff}$ decreases by the modification of the LC orientation on the membrane due to the elastic penalty imposed by the fluctuating membrane. This is due to the strong interaction between the LC and the membrane through the anchoring. Such behaviors have been explained by analyzing a model coarse-grained free energy with higher order terms in the fluctuations of the membrane shape and the LC directors. In our future work, we will study the effect of the anchoring on the membrane deformation in an LC-confined spherical membrane system. In such a case, much larger system is needed. Because a simulation on such a large system is demanding large computer power, we proposed a continuum model system to analyze the physical properties on the coarse-grained level.

ACKNOWLEDGMENTS

This work is partially supported by a Grant-in-Aid for Scientific Research (Grant No. 26287096) from the Ministry of Education, Culture, Sports, Science and Technology (MEXT), Japan.

[1] P. G. de Gennes and J. Prost, *The Physics of Liquid Crystals* (Oxford University Press, Oxford, 1993).
[2] J. K. Gupta, J. S. Zimmerman, J. J. de Pablo, F. Caruso, and N. L. Abbott, Langmuir **25**, 9016 (2009).
[3] I. H. Lin, D. S. Miller, P. J. Bertics, C. J. Murphy, J. J. de Pablo, and N. L. Abbott, Science **332**, 1297 (2011).
[4] D. Hartono, C. Y. Xue, K. L. Yang, and L. Y. L. Yung, Adv. Funct. Mater. **19**, 3574 (2009).
[5] T. Bera, J. Deng, and J. Fang, J. Phys. Chem. B **118**, 4970 (2014).
[6] S. H. Yoon, K. C. Gupta, J. S. Borah, S. Y. Park, Y. K. Kim, J. H. Lee, and I. K. Kang, Langmuir **30**, 10668 (2014).
[7] L. N. Tan and N. L. Abbott, J. Coll. Int. Sci. **449**, 452 (2015).
[8] M. G. Tomilin, S. A. Povzon, A. F. Kurmashev, E. V. Gribanova, and T. A. Efimova, Liq. Cryst. Today **10**, 3 (2001).
[9] M. Khan and S. Y. Park, Sens. Act. B Chem. **202**, 516 (2014).
[10] F. Caruso and H. Mohwald, J. Am. Chem. Soc. **121**, 6039 (1999).
[11] C. C. Muller-Goymann, Eur. J. Pharm. Biopharm. **58**, 343 (2004).
[12] L. Jia, A. Cao, D. Levy, B. Xu, P. A. Albouy, X. Xing, M. J. Bowick, and M. H. Lishchuk, Soft Matter **5**, 3446 (2009).
[13] S. I. Hernandez, J. A. Moreno-Razo, A. Ramirez-Hernandez, E. Diaz-Herrera, J. P. Hernandez-Ortiz, and J. J. de Pablo, Soft Matter **8**, 1443 (2012).
[14] J. Elgeti and F. Schmid, Eur. Phys. J. E **18**, 407 (2005).
[15] U. Seifert, Adv. Phys. **46**, 13 (1997).
[16] E. Kadivar, C. Bahr, and H. Stark, Phys. Rev. E **75**, 061711 (2007).
[17] X. Feng and C. Bahr, Phys. Rev. E **84**, 031701 (2011).
[18] X. Feng, A. Mourran, M. Moller, and C. Bahr, Soft Matter **8**, 9661 (2012).
[19] P. Sheng, Phys. Rev. A **26**, 1610 (1982).
[20] A. D. Rey and E. E. Herrera-Valencia, Soft Matter **10**, 1611 (2014).
[21] H. Stark, J. Fukuda, and H. Yokoyama, J. Phys. Cond. Matt. **16**, 1911 (2004).
[22] A. D. Rey, Langmuir **22**, 3491 (2006).
[23] J. G. Gay and B. J. Berne, J. Chem. Phys. **74**, 3316 (1981).
[24] D. J. Cleaver, C. M. Care, M. P. Allen, and M. P. Neal, Phys. Rev. E **54**, 559 (1996).
[25] R. Goetz and R. Lipowsky, J. Chem. Phys. **108**, 7397 (1998).
[26] E. de Miguel and C. Vega, J. Chem. Phys. **117**, 6313 (2002).
[27] S. J. Marrink and A. E. Mark, J. Phys. Chem. B **105**, 6122 (2001).